AIAA JOURNAL
Vol. 41, No. 6, June 2003

Navier–Stokes and Direct Simulation Monte Carlo Predictions for Laminar Hypersonic Separation

Christopher J. Roy,* Michael A. Gallis,† Timothy J. Bartel,‡ and Jeffrey L. Payne§
Sandia National Laboratories, Albuquerque, New Mexico 87185

Axisymmetric direct simulation Monte Carlo (DSMC) and Navier–Stokes simulations are performed as part of a code validation effort for hypersonic flows. The flowfield examined herein is the Mach 11 laminar flow over a 25–55-deg blunted biconic. Experimental data are available for surface pressure and heat flux at a Knudsen number $Kn = 0.019$ based on the nose radius. Simulations at a reduced freestream density ($Kn = 0.057$) are performed to explore the region of viability of the numerical methods for hypersonic separated flows. A detailed and careful effort is made to address the numerical accuracy of these simulations, including iterative and grid convergence studies for Navier–Stokes and temporal, grid, and particle convergence studies for DSMC. Good agreement is found between the DSMC and Navier–Stokes simulation approaches for surface properties as well as velocity profiles within the recirculation zone for the reduced density case. The results obtained indicate that the failure of earlier DSMC simulations at $Kn = 0.019$ is due to insufficient grid refinement within the recirculation zone. Furthermore, it is shown that accurate simulations of the biconic at the experimental conditions with the DSMC method are not yet possible due to the extreme computational cost.

Nomenclature

d	=	molecular diameter, m
f	=	general solution variable
Kn	=	Knudsen number based on nose radius, λ/R_N
L	=	characteristic length scale, m
n	=	number density, particles/m^3
p	=	pressure, N/m^2, order of accuracy
q	=	heat flux, W/m^2
R	=	specific gas constant, 296.8 for N_2, J/kg · K
Re	=	Reynolds number, $\rho V L/\mu$
R_N	=	nose radius, 0.00635 m
r	=	grid refinement factor
T	=	translational temperature, K
t	=	time, s
u	=	axial velocity component, m/s
V	=	velocity magnitude, m/s
x	=	axial coordinate, m
y	=	radial coordinate, m
γ	=	ratio of specific heats
λ	=	mean free path, $1/[\sqrt{2}\pi d_{\text{ref}}^2 n(T_{\text{ref}}/T)^{\omega-1/2}]$, m
μ	=	absolute viscosity, N · s/m^2
ρ	=	density, kg/m^3
τ	=	wall shear stress, N/m^2
ω	=	temperature exponent for viscosity coefficient

Subscripts

k	=	mesh level, 1, 2, 3, fine to coarse
RE	=	Richardson extrapolation value
ref	=	reference value

Received 26 April 2002; revision received 15 November 2002; accepted for publication 24 January 2003.

*Senior Member of Technical Staff, Mail Stop 0825, Post Office Box 5800; cjroy@sandia.gov. Senior Member AIAA.
†Member of Technical Staff, Mail Stop 0827, Post Office Box 5800; magalli@sandia.gov. Member AIAA.
‡Principal Member of Technical Staff, Mail Stop 0820, Post Office Box 5800.
§Principal Member of Technical Staff, Mail Stop 0825, Post Office Box 5800. Member AIAA.

Introduction

THE performance of airbreathing propulsion systems for hypersonic vehicles can be greatly influenced by the interaction of an internally produced shock wave with a boundary layer.[1] In addition to the high thermal loads that can occur in the shock/boundary-layer interaction region, the adverse pressure gradients can lead to flow separation, significantly reducing the effectiveness of control surfaces. Despite the significance of such flow phenomena, the mechanisms by which thermochemical nonequilibrium and real-gas effects influence the extent of the separation zone are not well understood. To enhance the understanding of such flows, experimental and computational studies have been promoted by the North Atlantic Treaty Organization's Research and Technology Organization (RTO).

RTO Working Group 10, Subgroup 3, was established in 1998 to address issues dealing with computational fluid dynamics (CFD) validation for hypersonic flight.[2] As part of this effort, Holden and co-workers[3–5] conducted experiments on two axisymmetric configurations where shock/boundary-layer and shock/shock interactions occur. The first configuration studied was an axisymmetric hollow cylinder flare with a sharp leading edge. The second configuration was a 25–55-deg biconic with a combination of blunt and sharp nosetips. The biconic was considered the more challenging of the two configurations because the shock/shock and shock/boundary-layer interactions were stronger for this case. All of the experiments were conducted at Reynolds numbers low enough to ensure that the flow remained laminar both upstream and downstream of the recirculation zone. For the numerical contributions to this validation study, several direct simulation Monte Carlo (DSMC)[6–8] and Navier–Stokes codes were employed.[6,9–12]

The results of this validation exercise were presented at the 39th AIAA Aerospace Sciences Meeting in January 2001 in the form of a blind comparison between the simulation predictions and the experimental data.[13] Two main issues arose as a result of this validation study. First, the computed surface heat fluxes (and, to a lesser extent, the surface pressures) were consistently higher than the experimental data in the attached flow region upstream of the separation point. Second, whereas the Navier–Stokes codes generally predicted the size of the recirculation zone in agreement with the experimental data, the DSMC approaches tended to underpredict the size of the recirculation region. The first issue was addressed in Ref. 6, where the sensitivity of the surface heating and pressure to vibrational excitation levels in the freestream were examined. It was later shown that the overprediction of the forecone heating is primarily due to

the effects of vibrational excitation in the hypersonic nozzle on the freestream conditions.[6,14,15]

The primary goal of this paper is to address the second issue: the underprediction of the recirculation zone size with DSMC relative to the Navier–Stokes simulations and the experimental data. To lessen the computational burden on the DSMC method, the density is lowered by a factor of three from the experimental values. In the absence of experimental data for this rarefied case, the issues associated with the underprediction of the recirculation zone with DSMC will be examined by a code-to-code comparison between DSMC and Navier–Stokes. This comparison is performed systematically with established verification principles.

In the definition currently accepted by the engineering community,[16,17] verification addresses the mathematical correctness or numerical accuracy of a simulation code and the subsequent numerical predictions. Verification deals purely with the mathematics of a chosen modeling scheme. Validation, on the other hand, usually entails a comparison to experimental data (i.e., real world observations) with carefully quantified uncertainty bounds, to ensure that the appropriate physical phenomena are adequately addressed by the simulation.

The verification process can be divided into two main categories: code verification and solution verification.[16–19] Code verification involves building confidence that the code is solving the governing equations correctly. There are a number of activities that fall under the heading of code verification. (See, for example, Refs. 16–19.) However, this work focuses on a code-to-code comparison between DSMC and Navier–Stokes. An important factor in performing such comparisons is that the transport models, thermodynamic models, and boundary conditions must be consistent between the two codes. Solution verification is the process by which the numerical accuracy of the solutions are assessed. For continuum mechanics codes, solution verification includes assessing the errors due to incomplete iterative convergence[20] (for steady-state problems), temporal convergence (for unsteady problems), and grid convergence.[21] For particle-based codes, solution accuracy includes assessing temporal convergence, grid convergence, and particle convergence.

The remainder of this paper is arranged as follows. The first section provides details on the two simulation approaches employed, including the careful choice of submodels and boundary conditions to insure a consistent code-to-code comparison. The second section includes simulation predictions from the blind validation study,[6] along with the subsequently released experimental data.[13] In the third section, the discrepancies regarding the size of the recirculation zone for the DSMC predictions are addressed by performing comparisons between DSMC and Navier–Stokes for the experimental biconic geometry at a reduced freestream density. Conclusions are presented in the final section.

Simulation Approaches

DSMC

The particular DSMC method used in this study is that of Bird[22]; the massively parallel processor implementation, Icarus, is described by Bartel et al.[23] In brief, the DSMC method is applied as follows. The computational domain is populated with "computational molecules," each of which typically represents a large number of identical real molecules or atoms (e.g., 10^{10}). During one time step, computational molecules move from one location to another, interact with boundaries, experience collisions, and are sampled to accumulate statistics. During a move, computational molecules travel at constant velocity for the entire time step or until a boundary is encountered. In the latter situation, the appropriate boundary condition is applied and the remaining portion of the time step is completed.

Typical boundary conditions are inflow (computational molecules entering the domain with a prescribed Maxwellian distribution), outflow (computational molecules crossing this boundary being deleted, appropriate for supersonic applications), diffuse wall (computational molecules are reflected with a prescribed Maxwellian distribution), and specular wall (computational molecules being reflected with mirror symmetry).

Following movement and boundary interactions, computational molecules experience collisions that change their velocities. Note that computational molecules have three-dimensional velocity vectors for collision purposes, even if a two-dimensional geometry is considered. After the collision phase, statistics (for example, number density, velocity, and temperature) are accumulated on the computational mesh, which exists only for this purpose and for determining possible collision pairs. To preclude nonphysical behavior, the mesh cell spacing is constrained to be less than one-third of a local mean free path and the characteristic length scale based on local flow gradients. The time step is similarly constrained to less than a mean collision time.[22]

The Icarus DSMC code was written for massively parallel computing environments to allow for the extreme computational requirements of the DSMC method.[23] For computational efficiency, the Icarus code uses body-fitted, multiregion meshes. Code verification studies have been performed that compare DSMC simulations to well-established theoretical results. (For example, see Refs. 24 and 25.) The DSMC simulations in the present work were performed on the 4500 node (9000 processor) ASCI Red platform (330-MHz Pentium II processors) using 1024 processors for 24 h each.

Navier–Stokes

The Navier–Stokes code is the Sandia Advanced Code for Compressible Aerothermodynamics Research and Analysis (SACCARA). This code was developed from a parallel distributed memory version[26,27] of the INCA code, originally written by Amtec Engineering. The SACCARA code is used to solve the Navier–Stokes equations for conservation of mass, momentum, and energy in axisymmetric form. The governing equations are discretized using a cell-centered finite volume approach. The convective fluxes at the interface are calculated by the use of the Steger–Warming[28] flux vector splitting scheme. Second-order reconstructions of the interface fluxes are obtained via MUSCL extrapolation.[29] A flux limiter is employed that reduces to first order in regions of large second derivatives of pressure and temperature. This limiting is used to prevent oscillations in the flow properties at shock discontinuities. The viscous terms are discretized using central differences.

The SACCARA code employs a massively parallel distributed memory architecture based on multiblock structured grids. The solver is a lower–upper symmetric Gauss–Seidel scheme based on the works of Yoon and Jameson[30] and Peery and Imlay,[31] which provides for excellent scalability up to thousands of processors.[32] A number of code verification studies have been performed, including comparison to established numerical benchmark solutions[33] and code to code comparisons.[33,34] The Navier–Stokes simulations presented herein were run using a single 400-MHz processor of a Sun Enterprise 10,000 shared-memory machine. The fine grid run for the rarefied biconic required approximately 1800 h of single-processor run time to converge to machine zero in double precision.

Computational Submodels

The computational submodels employed in the "Blind Validation Comparison" section are reported in Ref. 6. These models account for vibrational nonequilibrium and molecular dissociation and were chosen to best match the physics found in the experiment. However, no experimental data exist for the reduced density biconic. The computational submodels for this case are simplified to ensure consistency in the comparison between the DSMC and Navier–Stokes approaches. A discussion of these simplified models follows.

The molecular model used for the DSMC code is the variable hard sphere (VHS) model by Bird with the parameters given in Ref. 22. The VHS model assumes that the cross section of a molecule increases as its energy increases, with the rate of change related to the coefficient of viscosity. The VHS model assumes an isotropic scattering in the center of mass frame of reference. The standard VHS constants were modified to better represent the viscosity coefficient in the temperature range of interest (1000–3000 K) (Ref. 6). The power law viscosity model used for both the DSMC and

Navier–Stokes simulations is

$$\mu = (T/T_{\text{ref}})^{\omega}\mu_{\text{ref}} \tag{1}$$

where $T_{\text{ref}} = 1000$ K, $\mu_{\text{ref}} = 3.975 \times 10^{-5}$ N·s/m^2, and $\omega = 0.64$. For the thermal conductivity, a constant Prandtl number of 0.74 was chosen for the Navier–Stokes simulations to match the effective conductivity in the DSMC approach.[22] For the thermodynamic models, the Navier–Stokes predictions used the perfect-gas assumption ($\gamma = 1.4$ and the gas constant for nitrogen), and the DSMC predictions employed a rotational relaxation number of unity (i.e., the mean free path for rotational energy exchange was set equal to that for the translational mode). For both simulation approaches, the vibrational energy modes were neglected.

Boundary Conditions

At the inflow boundary, the Navier–Stokes simulations fix the velocity, static pressure, and static temperature. In the DSMC runs, the number density is fixed along with Maxwellian distributions of velocity and temperature about the specified mean values. Both approaches employ axial symmetry about the x axis and supersonic outflow conditions, that is, extrapolation, at the outflow boundaries. At solid walls, the Navier–Stokes simulations use standard no-slip wall boundary conditions with a fixed wall temperature of 297 K, whereas the DSMC approach employs a diffuse reflection condition with 100% thermal accommodation. Diffuse reflection is the case of surface reflection where the momentum of the reflected molecule depends only on the surface properties. The effect of changing the thermal accommodation coefficient from 1.0 to 0.8 has been shown to have a negligible influence on the results,[35] at least for flows without freestream vibrational excitation. For blunted biconics without freestream vibrational excitation, the no-slip boundary condition used in the Navier–Stokes code is expected to be valid.[14]

Blind Validation Comparisons

This section reports numerical predictions by the authors[6] that were performed as part of a blind validation study, the results of which were reported in Ref. 13. The blind predictions of Ref. 6 are presented in this section along with experimental data for surface pressure and surface heat flux.[13] The specific case examined herein is case B55D, run 31 of Ref. 4, which has Mach 11 laminar flow of nitrogen over a spherically blunted 25–55-deg biconic. The radius of the blunted nose is $R_N = 0.00635$ m, and the Knudsen number based on this radius is 0.019. The nominal freestream and surface boundary conditions used for both the Navier–Stokes and DSMC codes are presented in Table 1. The gas is nitrogen, and the transport and thermal nonequilibrium models are discussed in detail in Ref. 6. This reference also contains a detailed validation of the transport models for the temperature range of interest (1000–3000 K) along with an assessment of the numerical error in the surface quantities. Because the thermal state at the test section was not specified, the rotational and vibrational temperatures are assumed to be in equilibrium with the translational temperature at 144 K. Note that in all of the results presented herein, the axial coordinate x is measured from the virtual nose tip of the sharp forecone.

Table 1 Freestream and boundary conditions

Parameter	Value
Mach number	11.3
Reynolds number	142,060/m
Knudsen number (based on R_N)	0.019
Stagnation temperature	3283 K
Stagnation enthalpy	3.9670×10^6 m^2/s^2
Stagnation pressure	3.6266×10^6 N/m^2
Velocity	2,764.5 m/s
Static temperature	144.4 K
Static pressure	21.99 N/m^2
Number density	1.103×10^{22} particles/m^3
Wall temperature	297.2 K

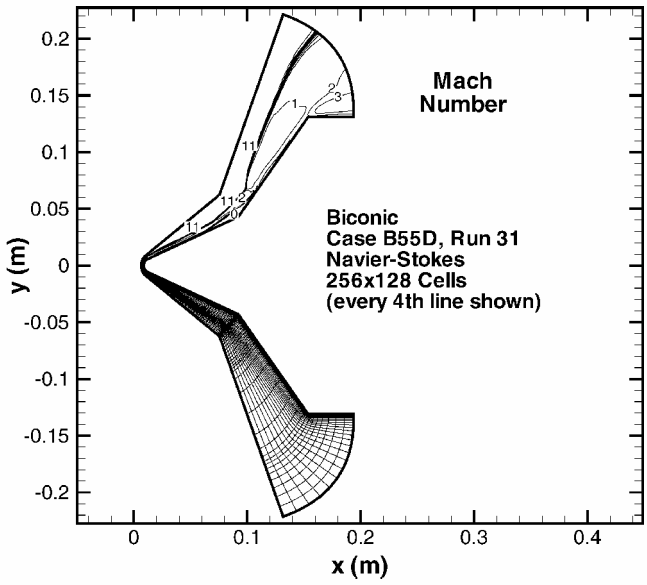

Fig. 1 Mach contours and Navier–Stokes grid for the biconic (case B55D, run 31 of Ref. 4).

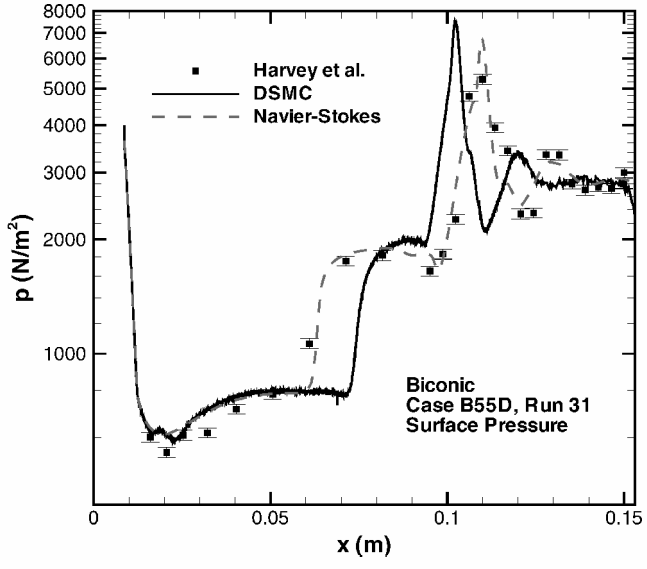

Fig. 2 Surface pressure distributions for the numerical predictions[6] along with experimental data from Ref. 13.

The general features of the axisymmetric flowfield are presented in Fig. 1, which shows Mach number contours (top) along with the Navier–Stokes grid mirrored across the symmetry line. A bow shock is produced in front of the spherically blunted nose and the 25-deg forecone. The presence of the 55-deg cone creates an Edney Type V shock/shock interaction,[10,11] which leads to flow separation upstream of the 25–55-deg juncture. Downstream of the shock/shock interaction, a complex series of shocks and expansions occur. The cylindrical portion of the domain ($x \geq 0.15$) is included only to provide a significant region of supersonic flow for the outflow boundary condition and is, thus, omitted from the results.

Comparisons between the surface pressure predictions from the two approaches and the experimental data are presented in Fig. 2. There is a significant rise in pressure at roughly $x = 0.05$ m, which denotes the beginning of the separation zone, followed by an additional rise in pressure near $x = 0.11$ m due to the shock/shock interaction. The Navier–Stokes predictions qualitatively match the experimental data, whereas the DSMC approach predicts a much smaller recirculation zone as judged by the rapid rise in pressure at approximately $x = 0.08$ m. Surface heat flux comparisons are given in Fig. 3. The two simulation approaches show good agreement for

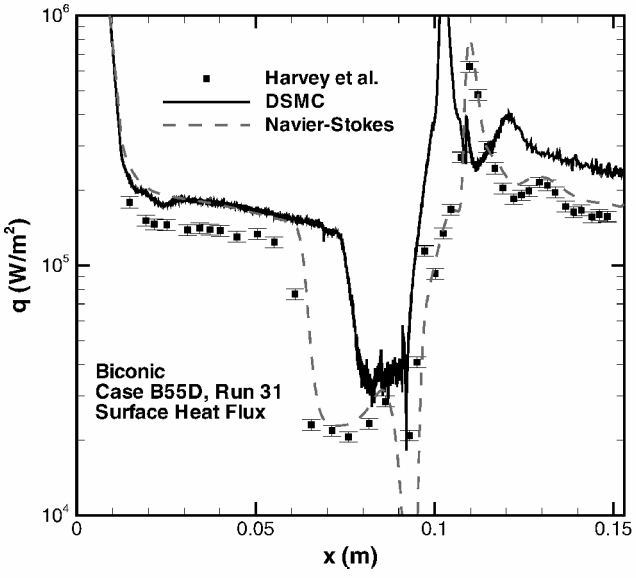

Fig. 3 Surface heat flux distributions for the numerical predictions[6] along with experimental data from Ref. 13.

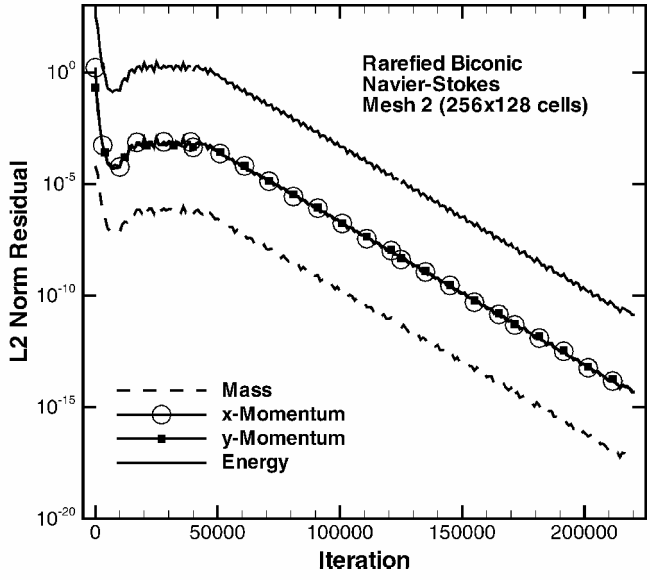

Fig. 4 Iterative convergence to steady-state for the rarefied biconic (Navier–Stokes).

the forecone heating, but significantly overpredict the heating relative to the experimental data. The Navier–Stokes predictions are consistently 25% higher on the forecone and 15% higher on the aft cone. The DSMC predictions are also approximately 25% higher than the data on the forecone and as much as 50% higher on the aft cone.

In the preceding comparison between the simulation results from Ref. 6 and the experimental data from Ref. 13, two basic questions arise: What is the source of the discrepancy in forecone heating between the simulations (which appear to agree) and the experimental data, and why does the DSMC method underpredict the size of the recirculation zone? These two trends were also observed by the other participants in the validation study. The first issue was addressed in detail by Candler et al.[14] and Holden et al.,[15] who compared simulations of the contoured D nozzle of the LENS I shock tunnel with pitot probe measurements across the test section. Their studies showed that vibrational freezing occurs downstream of the nozzle throat, thus modifying the freestream velocity and density from the values found by assuming thermal equilibrium. According to Candler et al.,[14] vibrational freezing in the nozzle appears to lower the surface heat flux and pressure by approximately 15 and 10%, respectively. They further showed that wall slip conditions could also affect the surface heating, especially in the presence of a vibrationally excited freestream. The second issue regarding the underprediction of the recirculation zone with the DSMC method is the focus of the current work. This question is answered in the following section by the application of the two simulation approaches to the study of the blunted biconic geometry, but with a reduced freestream density to lessen the computational burden on the DSMC method.

Rarefied Biconic

To explore the discrepancies in recirculation zone size between DSMC and Navier–Stokes, the blunted biconic geometry was computed with a reduced freestream density. The freestream density and pressure were reduced by a factor of three from the conditions given in Table 1 to explore grid, temporal, and particle convergence rigorously for the DSMC method. The DSMC method requires that the cell size be less than one-third of a mean free path,[22,36] thus, the reduction of the density by a factor of three reduces the required number of computational cells by roughly a factor of 10. For this rarefied case, the Knudsen number based on the nose radius ($R_N = 0.00635$ m) increases to 0.057, whereas the unit Reynolds number is reduced by a factor of three to 4.735×10^4/m. The simplified computational submodels discussed earlier were used to ensure consistency between the two approaches. The numerical accuracy of the Navier–Stokes simulations is verified by the performance of iterative and grid convergence studies, whereas the accuracy of the DSMC simulations are verified by examination of temporal, grid, and particle convergence.

Numerical Accuracy: Navier–Stokes

Iterative Convergence

The Navier–Stokes simulations were marched in pseudo-time until a steady state was reached. A steady state was assumed when the L2 norms of the residuals for all flow equations (mass, momentum, and energy) were reduced from their initial values by at least 12 orders of magnitude. The residual is evaluated by substitution of the current solution into the steady-state form of the discretized governing equations, that is, without the time derivatives. The residuals will approach zero as a steady-state solution is reached and the current solution satisfies the discretized form of the steady equations.

The L2 residual norms for a 256×128 cell biconic simulation are given in Fig. 4 for all four governing equations. The residuals are reduced by 12 orders of magnitude for each equation in approximately 200,000 iterations. Although the number of iterations is high, the diagonal point-implicit method has a computational cost per iteration similar to an explicit scheme. Although not shown, similar reductions in the residuals were found for the other grid sizes examined. The demonstrated reductions in residual norms give confidence that the iterative errors in the solutions are small and may be neglected relative to the grid convergence errors discussed hereafter.

Grid Convergence

Three meshes were used to estimate the grid convergence errors in the Navier–Stokes simulations of the rarefied biconic: mesh 1 (512×256 cells), mesh 2 (256×128 cells), and mesh 3 (128×64 cells). The Richardson extrapolation (RE) procedure is used to obtain a more accurate solution:

$$f_{\mathrm{RE}} = f_1 + \frac{(f_1 - f_2)}{r^p - 1} \tag{2}$$

where p is the observed order of accuracy of the numerical scheme. The medium and coarse grids were obtained from the fine grid by the elimination of every other grid line in each direction, thus, giving a grid refinement factor of $r = 2$. Although the theoretical order of accuracy of the SACCARA code is second order ($p = 2$), recent work has shown that the order of accuracy for multidimensional flows containing shock waves is reduced to first order ($p = 1$) on sufficiently refined meshes.[37,38]

Error estimates were obtained for the surface heat flux by comparison of the numerical solutions on each of the grids to the RE

Table 2 Recirculation zone characteristics for the rarefied biconic

Code	Grid	Cells[a]	Separation point x, m	Reattachment point x, m	Recirculation zone size, m
N–S[b]	Fine	512×256	0.079052	0.10111	0.022058
N–S[b]	Medium	256×128	0.079281	0.10112	0.021839
N–S[b]	Coarse	128×64	0.080652	0.10040	0.019748
DSMC	Fine	500×500	0.080356	0.10038	0.020024
DSMC	Medium	350×350	0.080655	0.10028	0.019625
DSMC	Coarse	250×250	0.081568	0.099804	0.018236

[a]Cells are given for region 3 only with the DSMC approach. [b]Navier–Stokes.

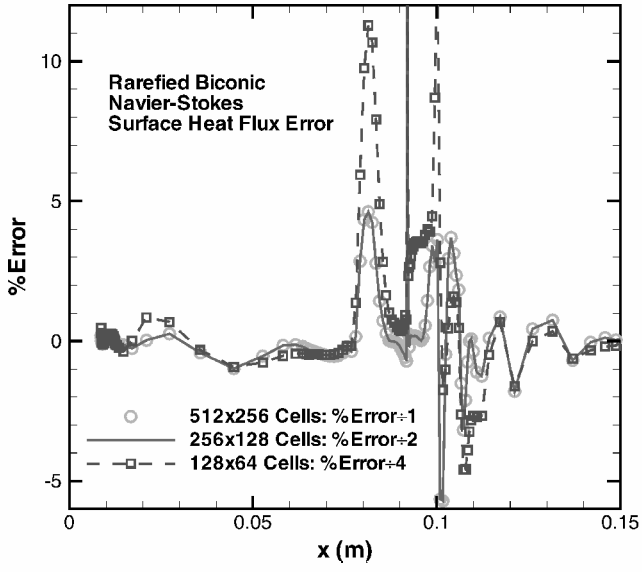

Fig. 5 Spatial error in the surface heat flux for the rarefied biconic (Navier–Stokes).

values, that is,

$$\%\,\text{error}\, f_k = 100\%(f_k - f_{\text{RE}})/f_{\text{RE}} \tag{3}$$

If the three solutions are all in the first-order asymptotic range, then the error on the three meshes will obey the following relationship:

$$\%\,\text{error}\, f_1 = \%\,\text{error}\, f_2/2 = \%\,\text{error}\, f_3/4 \tag{4}$$

The errors in surface heat flux are given in Fig. 5 for the three mesh levels normalized according to Eq. (4). Because Eq. (2) is used to estimate the exact solution, the normalized errors on mesh 1 and mesh 2 will, by definition, be equal. The solution on mesh 3 is employed to test whether all three meshes are in the first-order asymptotic range, that is, when Eq. (4) is satisfied. The three solutions are nearly asymptotic both upstream ($x \leq 0.08$ m) and downstream ($x \geq 0.1$ m) of the separation region. Within the recirculation zone, the three grids do not appear to be asymptotic. The grid convergence errors are generally below 1% for the finest mesh. The location of the beginning of the recirculation zone and the shock/shock interaction tend to move slightly as the mesh is refined; thus, the large spikes in the estimated error at 0.08 m and near 0.1 m are due to feature movement. The axial locations for separation point, reattachment point, and recirculation zone size are given in Table 2. The change in the recirculation zone size from the medium to fine meshes is less than 1%. Although not shown, the errors in the surface pressure were also generally below 1% along the surface.

To obtain conservative estimates of the grid convergence errors, a factor of safety should be included in the preceding error estimates. For example, in his grid convergence index, Roache employs a factor of safety of three when only two meshes are used.[21] For this case, three grids were used, and the order of spatial accuracy was observed to be approximately first order. Thus, a factor of safety of two is proposed for the rarefied biconic solutions. When the factor of safety is included, the estimated error in the surface heat flux is generally below 2%.

Numerical Accuracy: DSMC

To judge the numerical accuracy of the DSMC simulations, a variety of runs were made for the rarefied biconic geometry (Table 3). During the runs, the number of time steps, the mesh size, and the number of particles were independently varied to determine the effects on the solutions. The number of time-accurate time steps is indicated by the number of moves to steady state. The time window over which statistics were collected for postprocessing can be found by subtraction of the number of moves to steady state from the number of moves to the final state. For all simulations of the rarefied biconic presented herein, a global time step of $\Delta t = 5 \times 10^{-9}$ s was used. This time step was chosen such that the product of the local collision frequency and the time step was everywhere less than unity. A reduction of the time step to $\Delta t = 2.5 \times 10^{-9}$ s was found to have a negligible effect on the solution.

Statistical Steady State

One of the questions raised in a previous study[6] was whether the recirculation region formed near the junction between the two cones was stable and two dimensional. The experimental schlieren photographs[13] indicated that the recirculation zone was indeed two dimensional and steady in time. The DSMC simulations (runs 1–5 in Table 3) were marched in time to determine when a steady-state solution was reached. As noted in Table 3, runs 2–5 were restarted from their earlier runs, each one consisting of a 24-h run.

Surface heat transfer distributions for the reduced density biconic were obtained from 0.4 to 2 ms. The heat transfer was considered a good indicator of statistical convergence because the V^3 dependence takes longer to reach steady state than the pressure, which has a V^2 dependence. Figure 6 presents the evolution of the heat transfer with

Table 3 DSMC run summary for the rarefied biconic

Run	Particles per cell	Number of cells	Moves to steady state	Moves to final state	Restarted from run
1	12	995,000	70,000	80,000	——
2	12	995,000	70,000	80,000	1
3	12	995,000	70,000	80,000	2
4	12	995,000	70,000	80,000	3
5	12	995,000	70,000	80,000	4
6	24	995,000	20,000	40,000	5
7	7	865,000	70,000	80,000	——
8	12	865,000	70,000	80,000	7
9	7	805,000	70,000	80,000	——
10	12	805,000	70,000	80,000	9

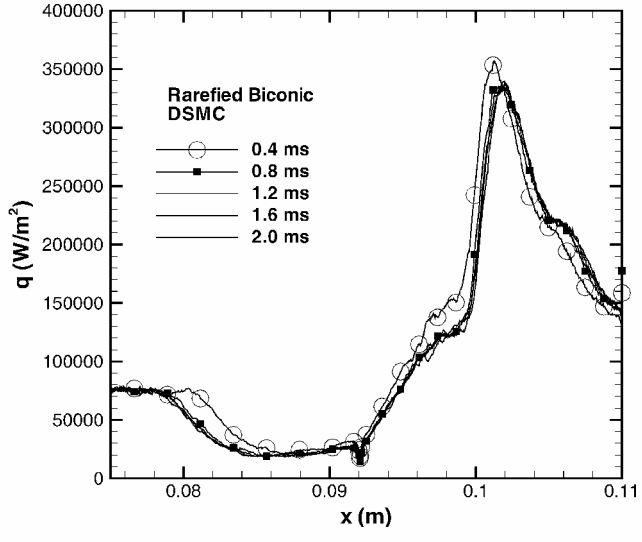

Fig. 6 Sensitivity of the surface heat flux to total simulation time for the rarefied biconic simulations with DSMC.

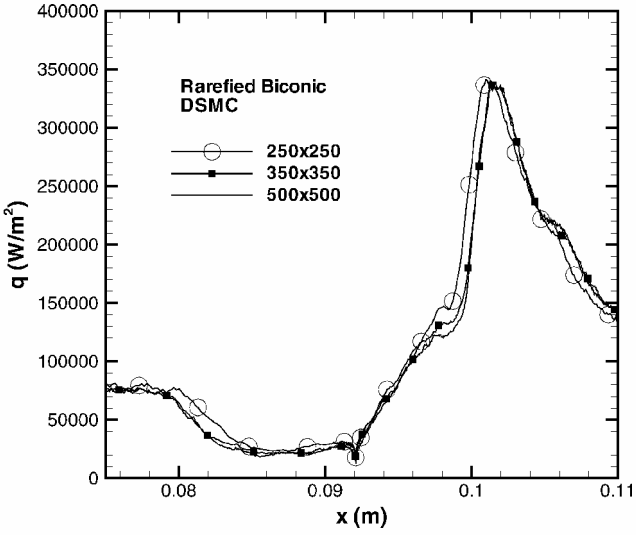

Fig. 7 Sensitivity of the surface heat flux to grid refinement in the recirculation zone for the rarefied biconic simulations with DSMC.

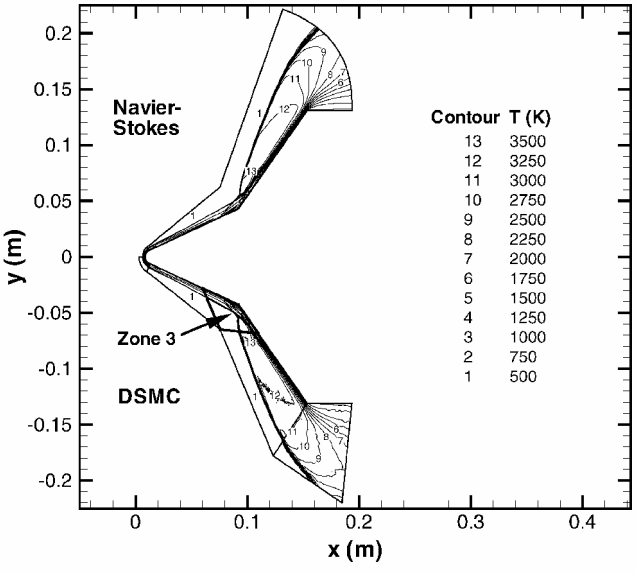

Fig. 8 Temperature contours for the rarefied biconic using Navier–Stokes and DSMC.

time for runs 1–5. Note that the axial scale has been increased to focus on the recirculation zone and shock/shock interaction region. Based on Fig. 6, a steady-state result was reached by 0.8 ms.

Grid Convergence

The sensitivity of the recirculation zone to grid resolution is examined in Fig. 7. A five-region mesh was used for the biconic that encompassed the entire recirculation zone within the third region. (See Fig. 8 for a schematic of the five regions.) Grids of 250 × 250 (coarse), 350 × 350 (medium), and 500 × 500 cells (fine) were used for the third region (runs 10, 8, and 2, respectively). The cell aspect ratio for this region was near unity. The grid sizes for the other regions were chosen based on an earlier grid refinement study performed on the forecone.[39] These runs were started from uniform initial conditions. The cell sizes in the recirculation zone were generally lower than one-third of a mean free path for the two finer grids, but not for the 250 × 250 cell grid. It is clear from Fig. 8 that the 350 × 350 and 500 × 500 cell meshes produced virtually identical results. The 500 × 500 mesh was used for the remainder of this study. By examination of the surface shear stress in this region, it was found that the size of the recirculation zone changed by 7.2% from the coarse to the medium mesh, but only 1.1% from the medium to the fine mesh. Quantitative information on the size of the recirculation zone is given in Table 2. Note that the size of the recirculation zone was underpredicted when there was insufficient grid refinement (coarse mesh). When the cell size is larger than $\lambda/3$ in the recirculation zone, the computational fluid viscosity is larger than the actual fluid viscosity.[36] From a physical point of view, the larger cell sizes allow collision partners to be selected from larger regions, thus, the collisions are felt over larger distances. This artificial viscosity dissipates the vortex energy and, thus, results in a smaller recirculation zone.

Particle Convergence

The effect of the number of particles on the predictions was also investigated. Reference 39 gives results for the surface heat flux after 2 ms of run time with an average of 12 and 24 particles per cell (runs 5 and 6, respectively). No difference in the behavior of the computed results was observed apart from a small reduction in the statistical noise. The reduction was small compared to the increase in the computational effort because doubling the number of particles reduces the statistical noise by only 40%. (The statistical noise is a function of the square root of the collected samples.)

Results

Figure 8 presents a field comparison between the Navier–Stokes and DSMC predictions for the temperature of the reduced density biconic. The DSMC results correspond to the 24-particle-per-cell, 2-ms case, where the fine mesh for the third region was used with a total of 995,000 cells (run 6). The Navier–Stokes results employed the finest mesh (512 × 256 cells). For both methods, the temperature increases from 144 K in the freestream to roughly 3800 K in front of the spherical part of the cone. A detached shock is developed that interacts with the shock formed in front of the second cone, creating a shock/shock interaction. The shock/shock interaction creates a maximum temperature of roughly 3500 K. Downstream of the shock/shock interaction, the temperature gradually drops until the end of the second cone. Good qualitative agreement is seen between the predictions of the two numerical schemes.

Figures 9a and 9b show pressure contours in the region of the shock/shock interaction for the Navier–Stokes and DSMC methods, respectively. Although the shock waves are clearly more diffuse in the case of the DSMC method, the two simulation approaches predict similar shock structures. The shock/shock interaction gives rise to a strong compression wave that impinges on the surface at approximately $x = 0.1$ m ($y = 0.055$ m). This impingement location corresponds to the peak surface pressure and heat flux locations shown in Figs. 10 and 11.

Figure 10 presents the predictions for the surface pressure along the biconic. The Navier–Stokes approach predicts the stagnation point ($x = 0.0087$ m) pressure to be approximately 1250 N/m^2, whereas the DSMC approach gives 1600 N/m^2. The reason for this discrepancy is the particle cloning required for the application of the DSMC method to axisymmetric flows, which results in artificially high pressure and heat flux in the first few cells near the stagnation point. The pressure predicted by both simulation approaches then rapidly drops to the forecone pressure of approximately 250 N/m^2. In the area of the recirculation zone, the pressure increases to roughly 750 N/m^2 and then reaches a maximum of almost 2000 N/m^2 in the area of the shock/shock interaction. A similar series of shocks and expansions are predicted with the two approaches downstream of the shock/shock interaction. With the exception of the stagnation point, good agreement is found between the two methods.

Similar behavior is observed for the surface heat flux (Fig. 11). After a maximum is achieved at the stagnation point, the heat flux drops along the first cone to approximately 1×10^5 W/m^2. The heat flux then drops significantly in the area of the recirculation zone to increase to a local maximum of about 3.5×10^5 W/m^2 in the area of the shock/shock interaction. The heat flux then drops rapidly along the second cone. Again, good agreement is found between the two approaches.

Figure 12 presents the shear stress along the surface of the biconic. The shear stress is zero at the stagnation point and then drops

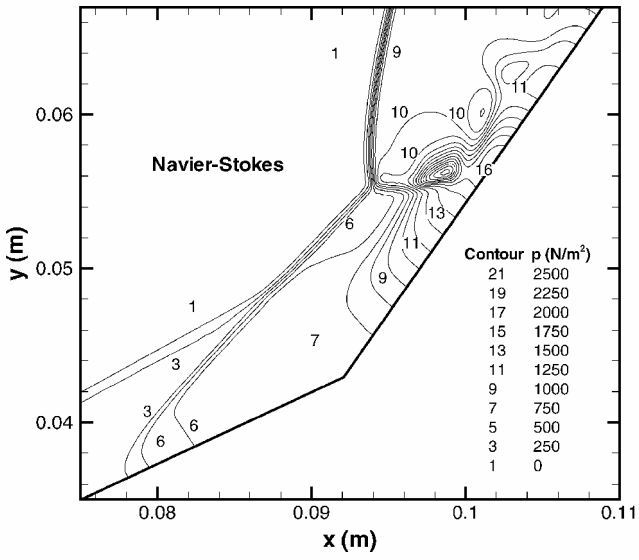

a)

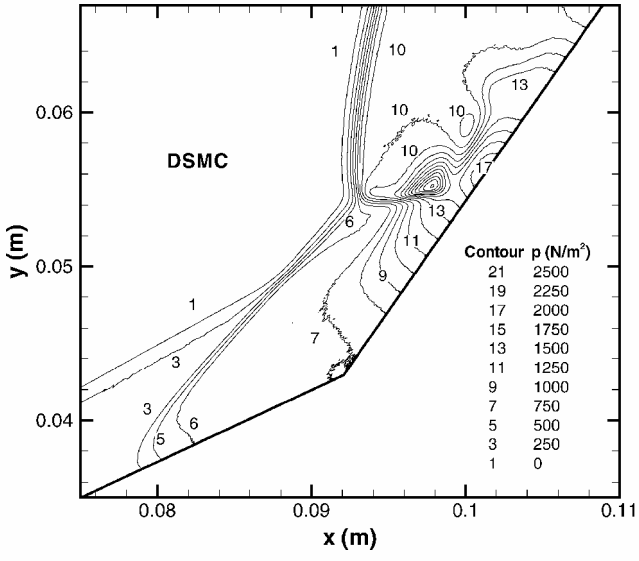

b)

Fig. 9 Pressure contours in the interaction region for the rarefied biconic using a) Navier–Stokes and b) DSMC.

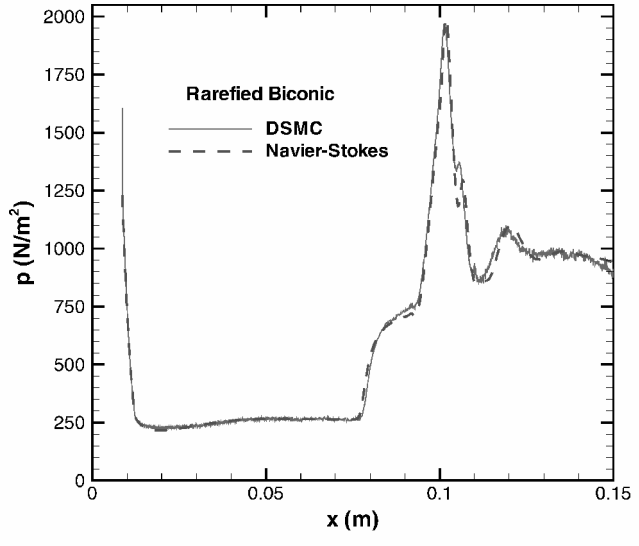

Fig. 10 Comparison of surface pressure predictions for the rarefied biconic using DSMC and Navier–Stokes.

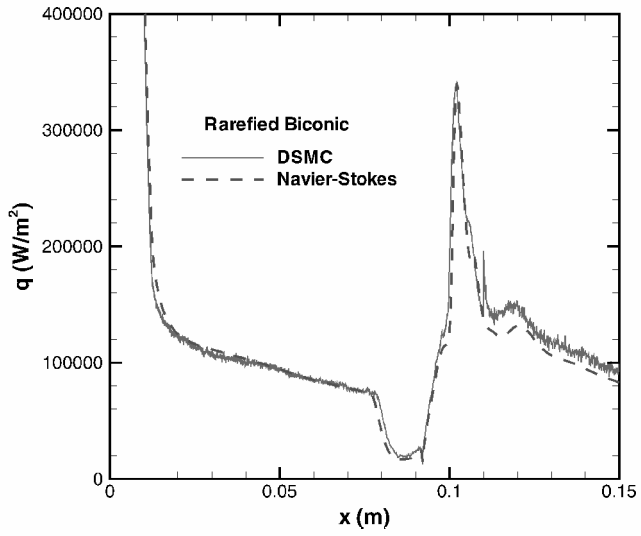

Fig. 11 Comparison of surface heat flux predictions for the rarefied biconic using DSMC and Navier–Stokes.

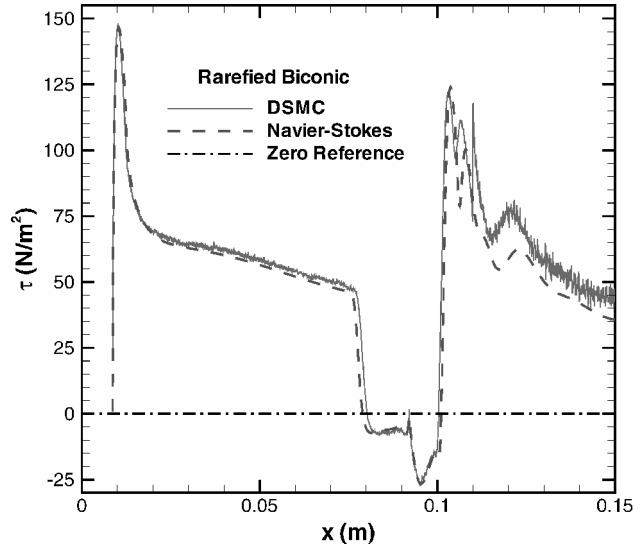

Fig. 12 Comparison of surface shear stress predictions for the rarefied biconic using DSMC and Navier–Stokes.

from 100 N/m^2 in the vicinity of the sphere/cone tangency point to about 60 N/m^2 along the surface of the forecone. A rapid drop at $x = 0.8$ m indicates the beginning of the recirculation zone that ends at $x = 0.1$ m. The numerical schemes are in good agreement both for the size and the structure of the recirculation zone. Despite the statistical noise of the DSMC solution, the local maximum and minimum at $x = 0.092$ and 0.095 m, respectively, show good agreement between the two methods. Discrepancies between the two approaches downstream of the shock/shock interaction region are likely due to the thicker shock waves predicted by the DSMC method.

The two simulation approaches show a difference of about 9% for the length of the recirculation region, with the Navier–Stokes approach providing the larger extent of separation. Based on the grid convergence studies of the preceding subsections, this difference does not appear to be a grid resolution issue. Lack of experimental data for this reduced density case does not allow one to draw conclusions about the validity of either of the predictions; however, some differences are expected because the DSMC method predicts a thicker, more realistic shock structure, and this flow is dominated by shock/boundary-layer and shock/shock interactions.

A qualitative assessment of the flowfield predicted by the two approaches is given in Fig. 13, which shows representative streamlines

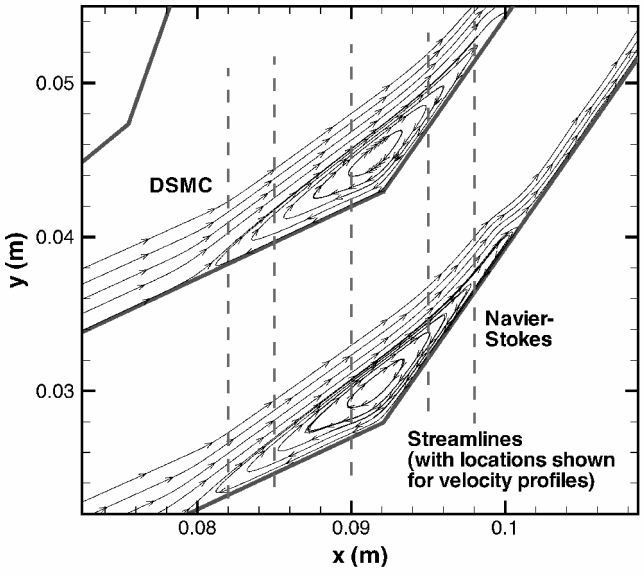

Fig. 13 Representative streamlines for the rarefied biconic using DSMC and Navier–Stokes.

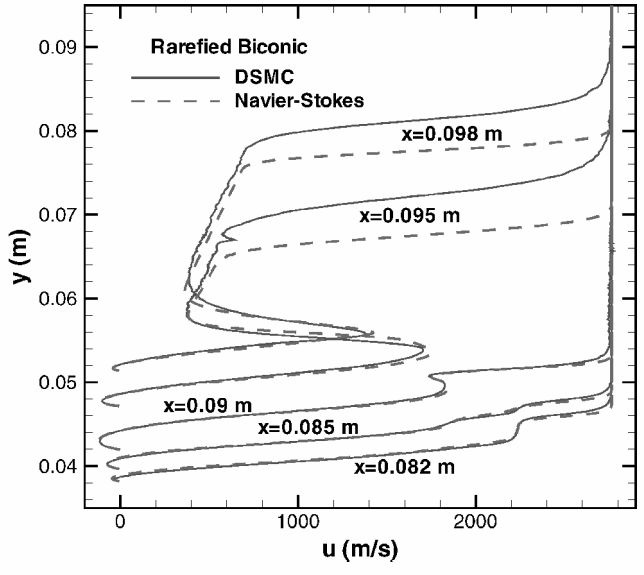

Fig. 14 Comparison of x equals constant profiles of axial velocity for the rarefied biconic using DSMC and Navier–Stokes.

in the recirculation zone. Good agreement is found between the two methods. Also shown in Fig. 13 are the axial locations where velocity profiles will be compared for the two methods. In Fig. 14, axial velocity profiles are given across the recirculation zone at $x = 0.082$, 0.085, 0.09, 0.095, and 0.098 m. At the first three stations, the two approaches predict similar structures. The difference becomes noticeable at the two downstream locations, with the DSMC solution predicting a thicker shock layer. This behavior is typical of DSMC codes in the area of the shock precursor where bimodal velocity distributions are obtained. The shock precursor is a highly nonequilibrium region where the freestream particles with a Maxwellian distribution interact with the postshock particles, which have a Chapman–Enskog distribution. This interaction results in collision rates and transport properties that are not accurately described by the continuum approach. Note that, even in these locations near the surface, where the density is higher, and, therefore, the equilibrium distributions assumed by the Navier–Stokes code are more accurate, the two schemes are in good agreement.

It has been shown that the DSMC and Navier–Stokes simulation approaches have achieved good agreement for the size and structure of this hypersonic shock-induced recirculation zone. Furthermore, the results of the DSMC grid convergence studies have shown that the size of the recirculation zone is underpredicted when there is insufficient grid refinement. We conclude, therefore, that the underprediction of the size of the recirculation zone with the DSMC method in the previous studies,[6–8,13] relative to both experiment and Navier–Stokes, is due to insufficient grid refinement. This same result was independently found in Ref. 40 by examination of the effects of grid refinement on a biconic at the experimental conditions.

The one-third of the mean free path rule can often be relaxed in regions free of strong gradients, without any visible effects on the results. However, Meiburg[41] and Bird[42] pointed out that in areas of high vorticity, the restriction of the cell size as a function of the mean free path becomes an important one. The selection of collision partners, the calculation of the collision frequency, and possibly the conservation of angular momentum within a cell appear to play a role in the accurate modeling of the separation zone where (as noted earlier) strong gradients in density, temperature, and velocity exist.

To apply the DSMC method[22] at the experimental conditions of case B55D, run 31, the number of particles would have to be increased by roughly an order of magnitude. Given the subsequent reduction in allowable time step, the computational effort would increase by approximately a factor of 30. Therefore, the computational resources to obtain a solution at the density found in the experiment would be prohibitive, even on today's fastest parallel computing platforms.

Conclusions

DSMC and Navier–Stokes simulations were performed for the Mach 11 laminar flow over a 25–55-deg blunted biconic geometry. The radius of the blunted nose was $R_N = 0.00635$ m, and the Knudsen number based on this radius was 0.019. Results were presented from a blind validation study[6] along with experimental data for surface pressure and heat flux from Ref. 13. One of the main issues that arose from the earlier validation study was that all DSMC simulations significantly underpredicted the extent of the separated flow region relative to the Navier–Stokes simulations and the experimental data.[6–8] These results bring into question the ability of the DSMC method to predict separated flows accurately. This issue is resolved in the current work by examination of the flow over the same blunted biconic geometry, but with a reduction of the freestream density by a factor of three. The density was decreased to reduce the computation burden on the DSMC method. Because no experimental data exist for these modified freestream conditions, the transport and thermochemical models were also simplified to improve the consistency between the DSMC and Navier–Stokes simulation approaches.

A rigorous study of the numerical accuracy was performed. For the Navier–Stokes simulations, the iterative convergence errors were shown to be small by the reduction of the L2 norms of the residuals for each conservation equation (mass, momentum, and global energy) by 12 orders of magnitude. The grid convergence errors in surface heat flux were assessed by the performance of simulations on three meshes (512×256, 256×128, and 128×64 cells). These errors were estimated to be less than 2% for the fine mesh, except where flow features, for example, separation point and shock/shock interaction, moved slightly with grid refinement. The accuracy of the DSMC simulations was assessed by independent variation of the total simulation time, the grid density in the recirculation zone, and the number of particles, with converged results obtained in each case.

A comparison between the DSMC and Navier–Stokes simulations of the rarefied biconic showed good agreement for both surface properties along the biconic and velocity profiles within the recirculation zone. The good agreement between the two simulation approaches suggests that the DSMC method is indeed capable of accurately predicting recirculating flows. Furthermore, the grid refinement study showed that the DSMC method underpredicted the size of the separated region on insufficiently refined meshes. These two results provide strong evidence that the reason for the underprediction of the recirculation zone with the DSMC method[22] in previous studies[6–8] was insufficient grid refinement in this region. It was shown that fully resolved DSMC simulations at the

experimental conditions are too computationally intensive for the computing resources currently available.

Acknowledgments

Sandia is a multiprogram laboratory operated by Sandia Corporation, a Lockheed Martin Company, for the U.S. Department of Energy under Contract DE-AC04-94AL85000. The authors thank Michael Holden of Calspan–University at Buffalo Research Center and John Harvey of Imperial College in London for providing the experimental data and for organizing this computational fluid dynamics validation study. We also thank Basil Hassan, David Kuntz, Dan Rader, and John Torczynski of Sandia National Laboratories, who provided thoughtful technical reviews of this work.

References

[1]Schlichting, H., *Boundary-Layer Theory*, 7th ed., McGraw–Hill, New York, 1979, pp. 358–372.

[2]Knight, D., "RTO WG 10: Test Cases for CFD Validation of Hypersonic Flight," AIAA Paper 2002-0433, Jan. 2002.

[3]Holden, M., "Experimental Studies of Laminar Separated Flows Induced by Shock Wave/ Boundary Layer and Shock/Shock Interaction in Hypersonic Flows for CFD Validation," AIAA Paper 2000-0930, Jan. 2000.

[4]"Experimental Database from CUBRC Studies in Hypersonic Laminar and Turbulent Interacting Flows Including Flowfield Chemistry," RTO Code Validation of DSMC and Navier–Stokes Code Validation Studies, Calspan–Univ. at Buffalo Research Center, Buffalo, NY, June 2000.

[5]Holden, M. S., and Harvey, J. K., "Code Validation Study of Laminar Shock/Boundary Layer and Shock/Shock Interactions in Hypersonic Flow, Part A: Experimental Measurements," AIAA Paper 2001-1031, Jan. 2001.

[6]Roy, C. J., Bartel, T. J., Gallis, M. A., and Payne, J. L., "DSMC and Navier–Stokes Predictions for Hypersonic Laminar Interacting Flows," AIAA Paper 2001-1030, Jan. 2001.

[7]Moss, J. N., "DSMC Computations for Regions of Shock/Shock and Shock/Boundary Layer Interaction," AIAA Paper 2001-1027, Jan. 2001.

[8]Boyd, I., "Monte Carlo Computations of Hypersonic Interacting Flows," AIAA Paper 2001-1029, Jan. 2001.

[9]Candler, G. V., "Navier–Stokes Predictions for Hypersonic Interacting Flows Including Air Chemistry," AIAA Paper 2001-1024, Jan. 2001.

[10]Gnoffo, P. A., "CFD Validation Studies for Hypersonic Flow Prediction," AIAA Paper 2001-1025, Jan. 2001.

[11]Wright, M. J., Sinha, K., Olejniczak, J., Candler, G. V., Magruder, T. D., and Smits, A. J., "Numerical and Experimental Investigation of Double-Cone Shock Interactions," *AIAA Journal*, Vol. 38, No. 12, 2000, pp. 2268–2276.

[12]Kato, H., and Tannehill, J. C., "Computation of Hypersonic Laminar Separated Flows Using an Iterated PNS Algorithm," AIAA Paper 2001-1028, Jan. 2001.

[13]Harvey, J. K., Holden, M. S., and Wadhams, T. P., "Code Validation Study of Laminar Shock/Boundary Layer and Shock/Shock Interactions in Hypersonic Flow, Part B: Comparison with Navier–Stokes and DSMC Solutions," AIAA Paper 2001-1031, Jan. 2001.

[14]Candler, G. V., Nompelis, I., Druguet, M.-C., Holden, M. S., Wadhams, T. P., Boyd, I. D., and Wang, W.-L., "CFD Validation for Hypersonic Flight: Hypersonic Double-Cone Flow Simulations," AIAA Paper 2002-0581, Jan. 2002.

[15]Holden, M. S., Wadhams, T. P., Harvey, J. K., and Candler, G. V., "Comparisons Between Measurements in Regions of Laminar Shock Wave Boundary Layer Interaction in Hypersonic Flows with Navier–Stokes and DSMC Solutions," AIAA Paper 2002-0435, Jan. 2002.

[16]*Guide for the Verification and Validation of Computational Fluid Dynamics Simulations*, G-077-1998, AIAA, Reston, VA, 1998, p. 3.

[17]"Editorial Policy Statement on the Control of Numerical Accuracy," *Journal of Fluids Engineering*, Vol. 115, No. 3, 1993, p. 340.

[18]Oberkampf, W. L., and Blottner, F. G., "Issues in Computational Fluid Dynamics Code Verification and Validation," *AIAA Journal*, Vol. 36, No. 5, 1998, pp. 687–694.

[19]Roache, P. J., *Verification and Validation in Computational Science and Engineering*, Hermosa, Albuquerque, NM, 1998.

[20]Roy, C. J., and Blottner, F. G., "Assessment of One- and Two-Equation Turbulence Models for Hypersonic Transitional Flows," *Journal of Spacecraft and Rockets*, Vol. 38, No. 5, 2001, pp. 699–710.

[21]Roache, P. J., "Perspective: A Method for Uniform Reporting of Grid Refinement Studies," *Journal of Fluids Engineering*, Vol. 116, No. 3, 1994, pp. 405–413.

[22]Bird, G. A., *Molecular Gas Dynamics and the Direct Simulation of Gas Flows*, Oxford Univ. Press, Oxford, 1994.

[23]Bartel, T. J., Plimpton, S., and Gallis, M. A., "Icarus: A 2-D Direct Simulation Monte Carlo (DSMC) Code for Multi-Processor Computers: User's Manual Version 10.0," Sandia National Labs., Rept. SAND 2001-2901, Albuquerque, NM, Oct. 2001.

[24]Gallis, M. A., and Torczynski, J. R., "The Application of the BGK Model in Particle Simulations," AIAA Paper 2000-2360, June 2000.

[25]Gallis, M. A., Torczynski, J. R., and Rader, D. J., "An Approach for Simulating the Transport of Spherical Particles in a Rarefied Gas Flow via the Direct Simulation Monte Carlo Method," *Physics of Fluids*, Vol. 13, No. 11, 2001, pp. 3482–3492.

[26]Wong, C. C., Blottner, F. G., Payne, J. L., and Soetrisno, M., "Implementation of a Parallel Algorithm for Thermo-Chemical Nonequilibrium Flow Solutions," AIAA Paper 95-0152, Jan. 1995.

[27]Wong, C. C., Soetrisno, M., Blottner, F. G., Imlay, S. T., and Payne, J. L., "PINCA: A Scalable Parallel Program for Compressible Gas Dynamics with Nonequilibrium Chemistry," Sandia National Labs., Rept. SAND 94-2436, Albuquerque, NM, April 1995.

[28]Steger, J. L., and Warming, R. F., "Flux Vector Splitting of the Inviscid Gasdynamic Equations with Applications to Finite Difference Methods," *Journal of Computational Physics*, Vol. 40, 1981, pp. 263–293.

[29]Van Leer, B., "Towards the Ultimate Conservative Difference Scheme. V. A Second Order Sequel to Godunov's Method," *Journal of Computational Physics*, Vol. 32, No. 1, 1979, pp. 101–136.

[30]Yoon, S., and Jameson, A., "An LU-SSOR Scheme for the Euler and Navier–Stokes Equations," AIAA Paper 87-0600, Jan. 1987.

[31]Peery, K. M., and Imlay, S. T., "An Efficient Implicit Method for Solving Viscous Multi-Stream Nozzle/Afterbody Flow Fields," AIAA Paper 86-1380, June 1986.

[32]Payne, J. L., and Hassan, B., "Massively Parallel Computational Fluid Dynamics Calculations for Aerodynamics and Aerothermodynamics Applications," *Proceedings of the 1998 HPC-CP/CAS Workshop*, NASA CP-1999-208757, 1999, pp. 111–116.

[33]Roy, C. J., McWherter-Payne, M. A., and Oberkampf, W. L., "Verification and Validation for Laminar Hypersonic Flowfields," AIAA Paper 2000-2550, June 2000.

[34]Payne, J. L., and Walker, M. A., "Verification of Computational Aerodynamic Predictions for Complex Hypersonic Vehicles Using the INCA™ Code," AIAA Paper 95-0762, Jan. 1995.

[35]Moss, J. N., and LeBeau, G. J., "Hypersonic Separated Flow Simulations Using DSMC," AIAA Paper 2002-0214, Jan. 2002.

[36]Alexander, F. J., Garcia, A. L., and Alder, B. J., "Cell Size Dependence of Transport Coefficients in Stochastic Particle Algorithms," *Physics of Fluids*, Vol. 10, No. 6, 1998, pp. 1540–1542.

[37]Carpenter, M. H., and Casper, J. H., "Accuracy of Shock Capturing in Two Spatial Dimensions," *AIAA Journal*, Vol. 37, No. 9, 1999, pp. 1072–1079.

[38]Roy, C. J., "Grid Convergence Error Analysis for Mixed-Order Numerical Schemes," *AIAA Journal*, Vol. 41, No. 4, 2003, pp. 595–604.

[39]Roy, C. J., Gallis, M. A., Bartel, T. J., and Payne, J. L., "Navier–Stokes and DSMC Simulations for Hypersonic Laminar Shock–Shock Interaction Flows," AIAA Paper 2002-0737, Jan. 2002.

[40]Gimelshein, S. F., Levin, D. A., Markelov, G. N., Kudryavtsev, A. N., and Ivanov, M. S., "Statistical Simulation of Laminar Separation in Hypersonic Flows: Numerical Challenges," AIAA Paper 2002-0736, Jan. 2002.

[41]Meiburg, E., "Comparison of the Molecular Dynamics Method and the Direct Simulation Monte Carlo Technique for Flows Around Simple Geometries," *Physics of Fluids*, Vol. 29, No. 10, 1986, pp. 3107–3113.

[42]Bird, G. A., "Direct Simulation of High-Vorticity Gas Flows," *Physics of Fluids*, Vol. 30, No. 2, 1987, pp. 364–366.

G. V. Candler
Associate Editor